

Letter of Transmittal

Peng Peng
327 Eddy St
Ithaca NY, 14850

To Whom it May Concern
Cornell University
MAE MEng Department
Cornell University 130 Upson Hall
Ithaca NY, 14850

To Whom it May Concern,

The report attached contains information on my MEng Project I worked on with students in the ECE department regarding a fully autonomous robotic platform and how peripheral structures can be attached to that platform so the final product can be used in applications such as household cleaning.

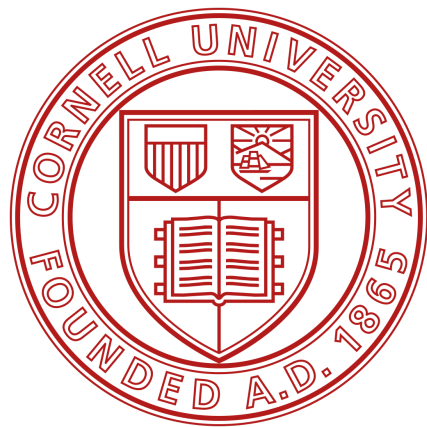
The full report will be submitted and released by the ECE MEng department. The work of my teammates as well as myself will be included in that report. However, this report contains the work for the parts I designed only. Specifically, this report will go over the casing of the robotic platform and a vacuum that can be attached to the platform that enables the robot to clean floors or other flat, dirty areas of a household. The report will contain design approaches and simulation analysis of the aforementioned components.

One thing of note is that during the 2020 semester, the COVID-19 pandemic required significant changes to project work. As a result, manufacturing and assembly of the components will not be achieved as fully as I would have wished otherwise, but no compromises have been made to the design and analysis portions of the work.

Best,
Peng Peng

Hardware Accelerated Autonomous Mobile Robot - Peripheral Hardware

Casing Structures and Vacuuming Applications



**Peng Peng
pp445
MEng Project Design Report**

Table of Contents

Letter of Transmittal	1
Table of Contents	3
Abstract	4
Executive Summary	5
Introduction	6
Background	7
Theory	8
Design	9
Analysis and Results	16
Discussion and Conclusion	21
References	22

Abstract

This project aims to create a mobile robot manipulator platform from scratch, and to develop all custom hardware and software designs. To achieve this goal, a team of ECE and MAE students have been assembled to accomplish all of the hardware and software engineering, as well as manufacturing. The final deliverable is a low-cost mobile robot that has a 6 DOF arm, capable of high speed SLAM, as well as vision-based navigation and pick-and-place. This is significant because there has not been open-sourced designs of similar form factor, and robotics enthusiasts can build from our design to have their own manipulator platform (or vacuum robot) for a fraction of the cost of the Kuka Youbot (\$30k). The hardware acceleration aspect comes with the main high level computer being the Nvidia Jetson Nano that has a 128-core Maxwell GPU, as well as the integration of FPGAs for various tasks.

Executive Summary

For our MEng Design Project for the School of Electrical and Computer Engineering, we worked on developing the hardware and software for a small but powerful open source autonomous mobile robot platform. The requirements are that it has to be relatively cheap to build, have enough computation power for simultaneous localization and mapping (SLAM) and computer vision, as well as carry enough stored energy for powering a ~200W electrical device. There are a few applications that this robot is aimed for. The first is a fully custom robot vacuum to perform cleaning tasks like that of the Irobot Roomba. This was inspired by our personal experiences with cleaning robots, which was less than satisfactory due to the simple sensors used and the unsophisticated algorithms that cause them to crash into furniture frequently. Therefore, we aimed to solve this problem by using advanced sensors such as a Lidar, with a customizable suite of navigation and path planning algorithms written under the Robot Operating System (ROS) framework. The second is an affordable manipulator platform carrying a 6 degree-of-freedom (DOF) robot arm. The arm was designed by one of the project members previously, and is powered by cheap but accurate serial servos. This platform enables learning and research at a significantly lower budget than before, compared to the Kuka Youbot.

To achieve these goals, we designed the hardware from the ground up. The mobile robot chassis was designed to be completely 3D printed in one piece, and the drivetrain relies on affordable NEMA 17 stepper motors tied to a belt reduction transmission for extra torque. The battery was custom designed and built out of 18650 cells salvaged from a Tesla Model S, and configured in a 4s5p arrangement for a total of 200Wh capacity. The battery management system was purchased, but the electrical drive system as well as the onboard power delivery circuitry were custom designed, and packaged onto a 4-layer printed circuit board (PCB) atop an Arduino Mega 2560 microcontroller (MCU). The MCU software is written in Arduino IDE for accessibility, but is powerful enough to realize a >50hz control loop, hardware health monitoring, and system safety controls. The MCU communicates to the high level computer, the Nvidia Jetson Nano, via serial, both receiving high frequency commands and sending back diagnostic information. On the Jetson Nano, we are able to run full scale Ubuntu and ROS, to enable easy integration of the Rplidar A1M8 and cameras for computer vision. In addition, we have built a manual remote control mode using Logitech joysticks, for debugging and development purposes.

Introduction

With the rapid increase of automation, it is now not uncommon to see robots in our daily lives. From service to cleaning robots, there exist many successful commercialization examples of this technology. In industry, robots have taken over traditionally dangerous and mundane tasks, such as assembling screws and welding vehicles. With an estimated global market of just under 40 billion dollars in 2019, the field of robotics has become very valuable to learn in this era. However, although many engineering programs now offer robotics courses, most lack hands-on work with actual robots due to the cost and complexity of setting up such devices. On the hobbyist market, there exist either affordable, but poorly designed robot platforms with limited functionality, or costly systems that are neither space-efficient nor user-friendly. This project aims to address these issues by presenting a completely open-source, expandable mobile robot platform that fits in the home as well as a research laboratory. With a 3D printer, the robot base costs as little as \$400, and is designed for easy-deployment and attachments in mind. By using stepper motors and belts for the drive system, we were able to leverage the existing 3D printing market for cheap components in both motors and the controllers. By using the Mega 2560 platform as the low-level controller, we enable more people to develop and change our base design, many of whom may have used Arduinos before but are daunted by proprietary microcontroller development environments. By using the Nvidia Jetson Nano, we further extend the accessibility goal by introducing full-scale Ubuntu in a single board computer (SBC) package, capable of running most software packages available on common desktop computers. Moreover, leveraging the built in 128-core Maxwell graphics processor unit (GPU), the Jetson Nano is able to accelerate neural network inference tasks by over 10 times compared to similar SBC solutions. Beyond these design implementations, we have also come up with custom attachments to address some specific use cases. For the robot vacuum, we have developed a computational fluid dynamics (CFD) optimized, 3D printed vacuum system powered by an electric ducted fan (EDF) commonly used in radio control aircraft. The large onboard battery is able to satisfy its power requirements, and in testing it performed even better than commercial solutions, due to our cyclonic dust separation design. For the manipulator, we integrated a 6 DOF mini robot arm onboard. In the final product, we were able to get the robot vacuum system to be fully functional, using both the lidar and camera system for SLAM. The arm works, but needs some additional development for control and path planning. This document is a record of the research and development process, discussing all the hardware design, manufacturing, testing, as well as software development and modification guidelines.

Background

Most modern day vacuums can be categorized into two types: regular bagged (or canister) vacuums or cyclonic vacuums.

For the regular bagged vacuum, an electric powered fan within (at the back of) the vacuum rotates, increasing the speed of the airflow and thus decreasing the pressure of air at the fan. The pressure difference between the fan location and the pressure at the inlet of the vacuum creates a suction force, carrying in air and dust/dirt from the nozzle of the vacuum to the inside. Once inside the vacuum, the air and dust particles do not settle immediately into the bag or canister. Rather, because the airflow is directed from the inlet at the nozzle to the outlet at the back of the fan, the air and dust particles have inertia and want to “ride the air” all the way to the fan exit. Therefore, all regular bagged vacuums have a HEPA filter located inside the vacuum to filter out the dust particles from the exiting air, preventing the dust sucked into the vacuum from spewing back out and negating all vacuuming efforts. However, the filter also hinders vacuuming efforts: as dust hits the filter and attaches to it, the accumulation of dust at the filter acts like a wall and prevents air from flowing across the filter, and thus the vacuum as effectively. This creates one of the most noticeable disadvantages of regular bagged vacuums - their suction ability gradually diminishes through use and the filter needs to constantly be replaced.

To alleviate this problem, Dyson combined the idea of using cyclones to remove dust with vacuum cleaners to create the cyclonic vacuum. The cyclonic vacuum, like the regular bagged vacuum, uses an electric fan to suck in air and dust. However, unlike the regular bagged vacuum, in which the direction of airflow is more “linear”, the cyclonic vacuum spins the air and dust, separating the two together by “flinging” the dust away from the air much like how the spin cycle of a washing machine separates water from clothes. After the dust separates from the air, it hits the walls of the dust bin compartment and is trapped inside while the remaining air is free to circulate within the compartment and eventually making its way to the outlet at the back of the fan. In cyclonic vacuum cleaners, a filter is still typically used and located near the outlet of the vacuum to prevent any fine dust particles that might not have been separated through the cyclone process from exiting back into the air, and the suction of ability of cyclonic vacuums will still diminish through use until the filter is replaced. However, because most of the particles, especially the large and heavy ones, have already been reduced from the air stream, the vacuum will remain effective without the filter needing to be replaced for longer.

Due to the aforementioned advantages of the cyclonic vacuum compared to the standard vacuum, the peripheral vacuum attached to the robotic platform will adhere to the cyclonic design.

Theory

The working principle that governs how cyclone function is centripetal force: $F_c = \frac{mv^2}{r}$ where m is the mass of the rotating object - air or dust particles in this case, v is the velocity in which they enter the cyclone and r is the radius of the dust bin. While the fan (outlet of the dust bin) is located at the center of the dust bin, the inlet to the dust bin (outlet of the nozzle) is located at the edge of the dust bin, and the direction of the airflow at this point is tangential to the circle of the dust bin. When the air dust mixture is carried into the cyclone, the air and dust particles are assumed to have roughly the same velocity. The circle in which they attempt to travel in also have the same radius. However, because dust particles are proportionally much heavier than air particles, the dust particles experience a greater centripetal force compared the air particles and are "flung" to hit the walls, which impedes further motion of the dust particles, while the air particles continue to spin in the cyclone until eventually reaching the outlet [1]. Another way to understand the problem is because dust particles have greater mass than air particles, they have greater inertia and are more likely to travel in a straight line following their original track after the tangential inlet rather than changing their trajectory to follow the curve of the dust bin, causing them to hit the dust bin walls. Due to centripetal force, the air will form an upward vortex from the inlet of the dust bin to the outlet while the dust will form a downward vortex with a larger radius from the inlet to the floor. This phenomenon is coined "double vortex" [2].

The motion impedance of the dust particles at the wall of the dust bin is further enhanced by the concept of no-slip condition, shown in the figure below, in which a viscous fluid is assumed to have no velocity relative to the boundary (the wall of the dust bin) due to shear stresses the wall exerts on the fluids.

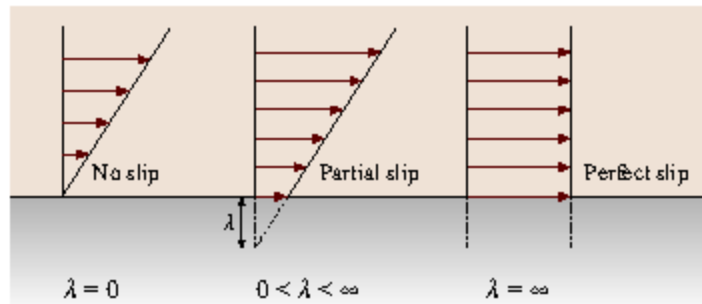


Figure 1. No Slip Condition [3]

Due to the no slip condition, once the airflow carrying the dust particles hits the wall, the particles "stick" to the wall and their velocities are greatly reduced, preventing them from traveling up to the filter and dust bin outlet.

Design

Before diving into the design of the cyclonic vacuum, a design for an enclosure for the robotic platform was necessary due to the abundance of wires leading from the power source to motor controller to motors and sensors and so on. The main purpose of the enclosure is to contain all the wires such that they would not “spill out” and get entangled in the spinning wheels. Furthermore, because enclosing the wires in a casing structure would make accessing ports and hardware more difficult, the enclosure would provide mounting for them.

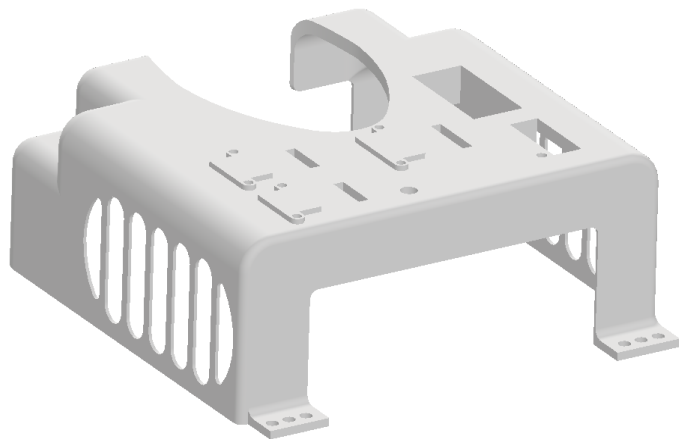


Figure 2. Enclosure

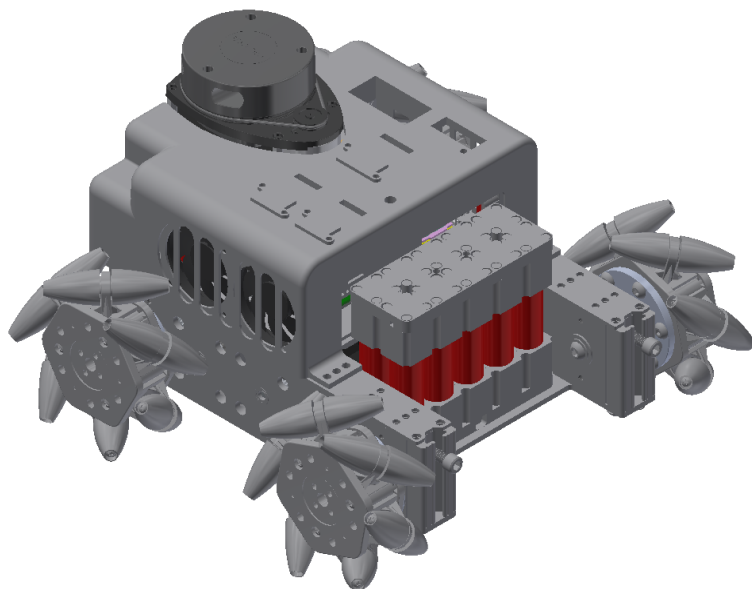


Figure 3. Enclosure in Main Assembly

The standalone enclosure and the overall assembly with the enclosure attached are shown in the figures above. The enclosure mounts to the chassis of the robotic platform via the roll of holes in the front and holes on the indent in the rear. Side mounting holes on the chassis exist at locations near the wheels but they are not used because the width of the screw head for bolting the enclosure would interfere with the rotations of the wheels. The thickness of the enclosure varies between the top and side faces. The side faces are 1.25mm thick as thicker would cause interference with the wheels and thinner would make the side faces flimsy and prone to snapping/breaking. The top face is slightly thicker than the side faces at 5mm to increase the structural integrity of the enclosure as there is more space available in the z-dimension. Two car grille-like openings on the enclosure exist on the side of the cooling fan and on the same location symmetric about the centerline of the chassis to act as inlets and outlets and help conduct airflow to the fans such that onboard components can be properly cooled to run efficiently. Meshing should be attached to the grille-like openings on both sides to filter out dust and dirt and prevent them from clogging the fan.

Six hardware components that the user can interface with are mounted to the enclosure. The three “z” shaped tabs are for cable plugs: two USBs for the keyboard and mouse and one HDMI for the display. The rectangular openings next to the z shaped mounts ensure that the cables can pass through the case. The hole below one of the cable mounts is allocated for a toggle switch that enables/disables the drivetrain. The rectangular opening with a small hole next to it to the right of the toggle switch is the mount for an OLED that displays the IP address, CPU and GPU usages. The OLED chip will mount from underneath the enclosure with the chip portion hidden by the enclosure and only the display showing through the rectangular opening and sitting flush to the top surface of the enclosure. The largest rectangular opening to the top of the OLED opening mounts a mechanical master kill switch for robot power. The master kill switch is shown in the figure below and has easily deflectable cantilever arm structures on the sides that protrude outwards in their naturally relaxed state and can easily bend inwards. To utilize this, the nominal opening of the rectangular mount is smaller than the max dimensions of the switch at its relaxed state such that the arms deflect when pushed into the opening and the friction holds it in place.



Figure 4. Master Kill Switch

Due to the thinness of the enclosure on its top surface and the need to use screws to mount the hardware, the plug mounts and master switch all have boss-like structures protruding inwards from the enclosure. For the plug mounts and toggle switch, the bosses provide length that allows for extra thread engagement, and for the master switch, the protrusion provides extra area to hold down the outward deflecting arms.

All parts of the enclosure, including the hardware that mounts to it, are below the plane of sight of the lidar.

The enclosure is manufactured through Cornell Rapid Prototyping Lab's (RPL) 3D printing services. Despite not having fillets can make the structure easier to print, fillets were included for aesthetic purposes and to reduce the likelihood of users cutting their hands on the case. Even though the design included fillets and overhang structures, the print quality from RPL was better than pre-envisioned. The final design went through two print iterations as the first iteration was too flimsy, leading us to increase the thickness to what it is now.

The final print iteration, assembled on the chassis, is shown in the picture below.

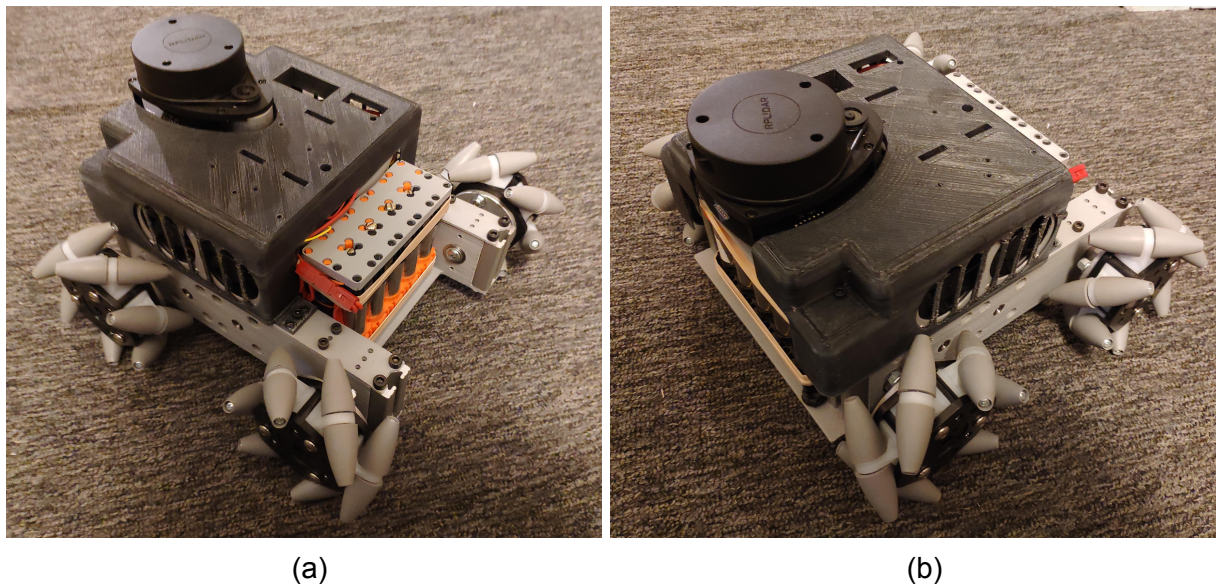


Figure 5 a&b. Enclosure Assembly Manufactured

The design of the cyclonic vacuum references existing cyclonic vacuums by Dyson and an online project called DIYson in which the designer tries to create a handheld vacuum similar to Dyson cyclonic vacuums without the expensive cost.

The selected fan that will power the vacuum and create suction is a 50mm EDF (electric duct fan) commonly used in radio control aircraft/ hobbyist aircraft and drones. The fan was selected based on its capability to create $\frac{1}{4}$ horsepower and 5N of thrust. To mount the EDF onto the

body of the dust bin, a fan sleeve has to be made due to the EDF's lack of mounting features. Due to the EDF having an extruding lip on one end and a very slight extruding ledge on the other, the diameter of the sleeve is slightly larger than the body diameter of the EDF and very slightly larger than the diameter of the extruding ledge. The sleeve also has a counterbore-like feature on one end to clear the extruding lip. To assemble the EDF into the shroud, the body of the EDF is first wrapped in paper to act as the shim to make up for its smaller diameter. Then the outside of the EDF and the inside of the sleeve are evenly coated with strong epoxy. The EDF slips into the sleeve ledge side first until the lip of the EDF is flush with the sleeve's bottom face and the epoxy should hold the structures in place. The assembly containing the EDF and sleeve is shown in the picture below.

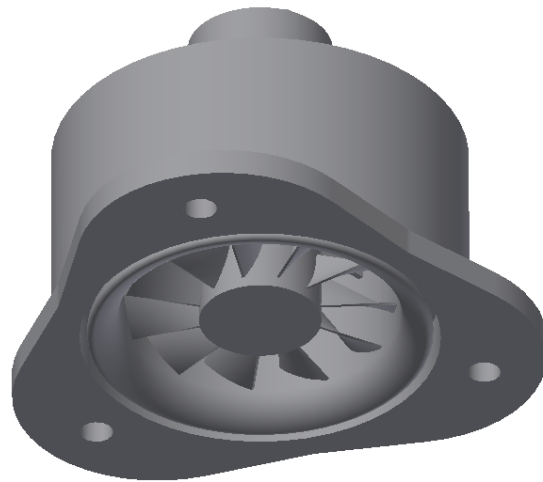


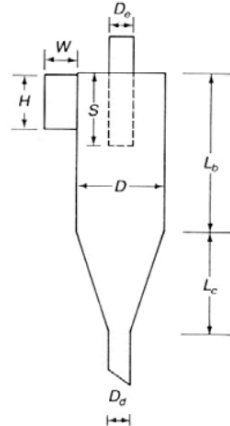
Figure 6. EDF Sleeve

The EDF will be mounted onto the top of the dustbin using the three mounting holes shown in the assembly figure.

The design of the dustbin references some cyclone design guidelines presented in an environmental engineering class at Dartmouth [4]. The diagram presented by the lecture slides of typical cyclone dimensions is shown in the figure below. The dustbin design tries to follow the guidelines for a high efficiency cyclone with some changes applied due to dimensional constraints.

Standard cyclone dimensions

Cyclone Type						
	High Efficiency	Conventional	High Throughput			
(1)	(2)	(3)	(4)	(5)	(6)	
Body Diameter, D/D	1.0	1.0	1.0	1.0	1.0	1.0
Height of Inlet, H/D	0.5	0.44	0.5	0.5	0.75	0.8
Width of Inlet, W/D	0.2	0.21	0.25	0.25	0.375	0.35
Diameter of Gas Exit, D_e/D	0.5	0.4	0.5	0.5	0.75	0.75
Length of Vortex Finder, S/D	0.5	0.5	0.625	0.6	0.875	0.85
Length of Body, L_b/D	1.5	1.4	2.0	1.75	1.5	1.7
Length of Cone, L_c/D	2.5	2.5	2.0	2.0	2.5	2.0
Diameter of Dust Outlet, D_d/D	0.375	0.4	0.25	0.4	0.375	0.4



SOURCES:
Columns (1) and (5) = Stairmand, 1951; columns (2), (4) and (6) = Swift, 1969; column (3) and sketch = Lapple, 1951.

Figure 7. Cyclone Design Dimensions [4]

The parameters “length of vortex finder”, “length of cone” and “diameter of dust outlet” does not apply in the dustbin design. The diameter of the gas exit is taken to be the diameter of the fan exit at 50mm. Following the ratios for high efficiency cyclones, the body diameter of the cyclone should be twice the diameter of the fan at 100mm. However, because we opted for using off-the-shelf filters for the vacuum with a max dimension of 80mm, 100mm would be too short when mounting is taken into consideration. While increasing the diameter of the body is not ideal because it would decrease the centripetal force, it would ease mounting concerns and increase the volume of dust the vacuum can hold, thus the body diameter is compromised at 130mm. According to the figure the width of the inlet (width of the dustbin nozzle) should be 20 percent of the body diameter bringing it to 26mm. The actual size of the width excluding the thickness of the nozzle is 24mm, close to the ideal. The height of the inlet and the length of the body are the two most compromised dimensions due to constraints from the chassis platform. The length of the body should be 1.5 times the diameter of the body at 195mm but the actual length of the body in this design is 80mm. If the body is any longer, the EDF, mounted on top of the dustbin would block the plane of vision of the lidar. Leaving the height at 80mm leaves a tight clearance of 2mm. The decreased length of the body also affects the height of the inlet. If the inlet was indeed half the diameter of the body it would be 65mm tall and almost as long as the body which is not ideal as then the inlet of air and dust would flow directly to the filter, clogging it faster than otherwise and negating the advantages of a cyclonic vacuum in the first place. Ideally, the nozzle would be pointed in the middle to lower portion of the dustbin body, allowing some time and distance for the airstream to travel ample rotations to shake off the dust. Moreover, because the goal of the vacuum is cleaning the household, the nozzle of the vacuum needs to be pointed downwards towards the floor. Unless the nozzle is designed to be

abnormally long extrusion, the geometry for a bend with such height is not physically possible. The compromised height of the inlet turned out to be quite far from the guidelines at 25mm.

Also according to the Dartmouth lecture, the number of revolution of the air traverses inside the body and cone of a cyclone follows the equation:

$$N = \frac{1}{H}(L_b + \frac{L_c}{2}) [4]$$

Where N is the number of turns, H is the height of the inlet duct, Lb is the length of the cyclone body and Lc is the length of the cyclone duct. Substituting in the design dimensions and assuming Lc = 0, the number of turns air should theoretically travel through inside the dustbin is 3.2.

The number of turns is important because like aforementioned, it makes intuitive sense that the more number of turns air traverses through, the more opportunities it has to spin off the dust particles it carries. According to the same presentation, the smallest diameter particle dp that can be separated by a cyclone if it starts at the inside edge of the inlet duct is:

$$d_p = \left[\frac{9\mu W}{\pi N V_i (\rho_p - \rho_a)} \right]^{\frac{1}{2}} [4]$$

Where μ is the viscosity of air, ρ_p is the density of the particle, ρ_a is the density of air, W is the width of the inlet duct and Vi is the inlet air velocity.

Solving for the smallest particle diameter requires solving for the inlet air velocity, which can be found using:

$$F = \dot{m}_e v_e - \dot{m}_i v_i + (p_e A_e - p_i A_i), \dot{m}_e = \rho_{air} v_e A_e, \dot{m}_i = \rho_{air} v_i A_i [5]$$

Where F is the thrust force generated by the EDF, \dot{m} is the mass flow rate at the inlet and outlet, v is the velocity, p is pressure at inlet and outlet and A is the area. The area of the inlet and outlet are based on the aforementioned geometries. However, for simplicity of simulation, the outlet area is chosen to be the area of the filter instead of the fan. The pressure at the inlet and outlet are assumed to both be atmospheric. For simplicity purposes, and because the designated fluid in the simulation described in the later session of the report is air only, the mass flow rate is assumed to be of air only (only uses the density of air) though in reality the mass flow rate will be a mixture of air and dust. The velocities at the inlet and outlet are assumed to be identical. Finally, although the EDF reports to generate as much as 5N of thrust, only 3N is used to account for losses and inefficiencies. Using the aforementioned assumptions and design dimensions, the calculated velocity for Vi in the equation above is 31.32 m/s.

Using the calculated velocity in the equation for smallest particle diameter, and assuming the viscosity of air at room temperature (25 degrees Celsius) is $1.849 * 10^{-5} \frac{kg}{ms}$ [6], and using the density of dust as $1.49 * 10^3 \frac{kg}{m^3}$ [7], the smallest diameter we theoretically obtain is $2.92 * 10^{-6} m$ ($2.92 \mu m$). The average size of dust particles, according to the WHO, ranges from $1-100 \mu m$ [8], thus this cyclonic vacuum should theoretically pick up and separate most of the dust particles found inside a regular household.

The assembly of the cyclonic vacuum is shown in the figure below. Ideally, the entirety of the dustbin compartment will be made from transparent plastic such as polycarbonate so the user can clearly see how much dust has collected inside. However, since the polycarbonate cannot be 3D printed (they are usually injection molded) and Cornell only has 3D printing easily accessible, only a part of the lid will be made out of laser cut clear acrylic instead and the body of the dustbin will be made of non-transparent ABS. A hole on the lid, made of clear material, will be glued onto the rest of the lid, made of non-transparent ABS, using epoxy.

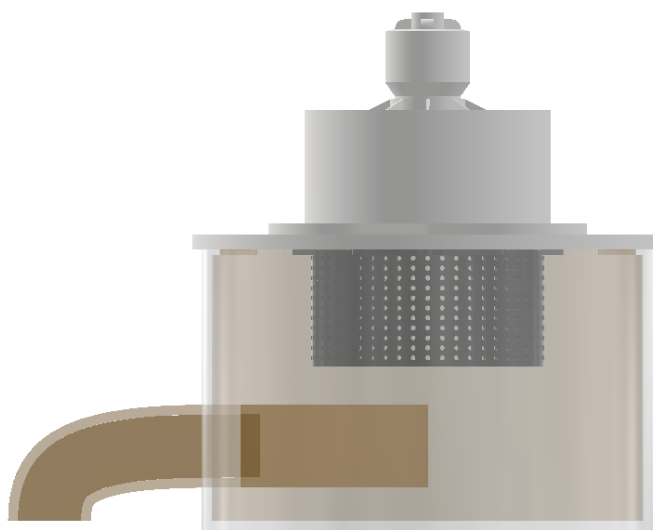


Figure 8. Cyclonic Vacuum Assembly

The lid of the dustbin and the body of the dustbin both have slots for disk magnets at their interface. There are a total of six magnets, each with a pull of 2 lbs, summing up to a total of 12 pounds, strong enough to handle the weight of the dust and dustbin itself but not too strong to prevent the user from pulling the lid off.

Analysis and Results

To visualize the trajectories of airflow inside the dustbin, make sure that an air vortex actually occurs and that the velocity of air and number of rotations we calculated is reasonable, we use CFD (computational fluid dynamics) to analyse the dustbin design. There are a variety of software programs we can utilize, but due to accessibility and familiarity, we have chosen ANSYS Fluent.

In order to use Fluent, a simplified model to represent the volume within the dustbin minus the volume of the filter was created as the fluid domain. All complex and unnecessary geometry such as the slots for the disk magnets are omitted for the ease of meshing. To capture the effects of the no slip boundary layer at the wall of the dustbin, inflation layers were used initially to create fine layers of mesh. However, inflation layers reduced the quality of mesh and led to poor convergence in the solution phase. To alleviate this issue, edge sizing around the top and bottom circle of the dustbin body and a small face sizing around the wall of the dustbin were implemented. The transition of the mesh was set to slow, meaning the mesh sizing would transition slowly from the extra fine sizing at the wall to the slightly coarser sizing inside of the volume domain to mimic the effects of inflation layers. Fine meshing is not utilized throughout the volume to minimize the solve time and computer memory usage. The final mesh, zoomed to show the equivalent effects of inflation layers, is shown in the figure below.

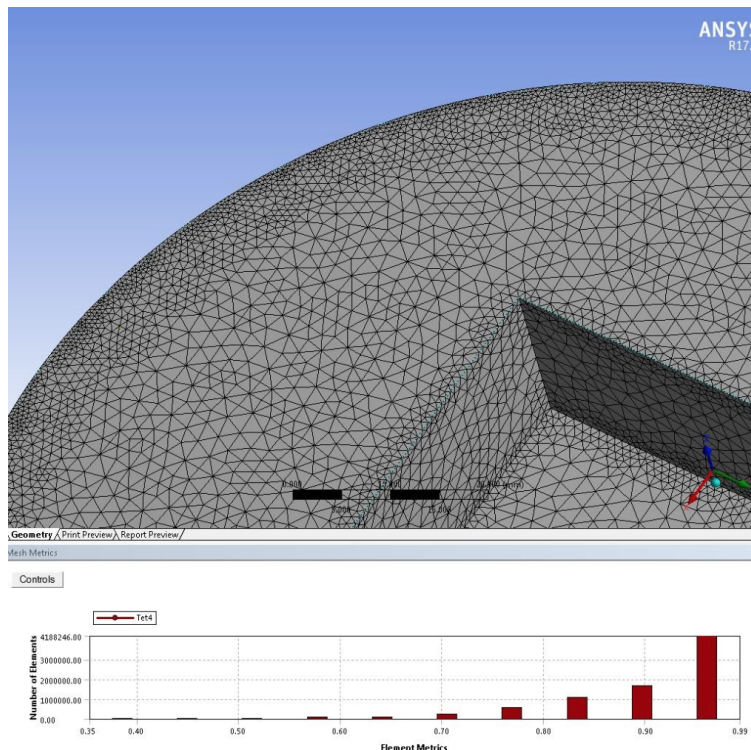


Figure 8. CDF Mesh

The bottom bar also pictured gauges the quality of the mesh. The mesh element metric displayed is orthogonal quality, which shows how close the angles between adjacent element faces are to some optimal angle determined by the program and mesh method. The quality ranges from 0 (bad, mesh is pretty much useless) to 1 (good, mesh is ideal). The mesh for the dustbin has an average orthogonal quality of 0.9 and a minimum of 0.32, a good statistic that will increase the chances of convergence when solving.

The boundary conditions of the inlet was chosen to be pressure inlet at atmospheric pressure; the boundary conditions of the dustbin wall was chosen as “wall” to signify the effects of the no-slip condition; the boundary conditions of the outlet was chosen as velocity outlet with a specified mass flow rate.

The mass flow rate at the exit is calculated from the aforementioned equation of $m_e = \rho_{air}v_eA_e$ and all aforementioned assumptions still hold. The specified mass flow rate is $0.119 \frac{\text{kg}}{\text{ms}}$.

The models/setup for the case ran is steady state, viscous, Spalart-Allmaras turbulent model. Steady state was chosen to visualize the behavior of the vacuum during a slightly prolonged time of use as household cleaning generally requires some time, and the Spalart-Allmaras model is chosen because it is a relatively simple, non-memory intensive one-equation model that is easier to lead to good convergence. The model was also designed specifically for aerospace applications involving wall-bounded flows, similar to the scenario with the cyclonic vacuum.

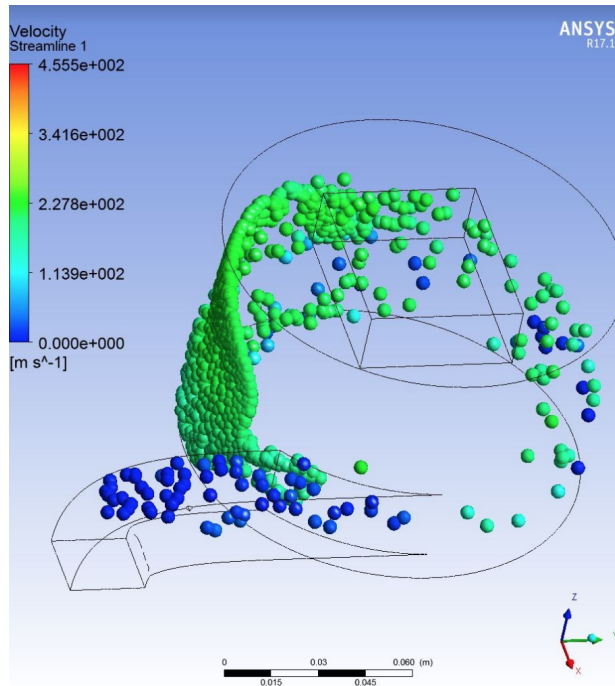


Figure 9. Streamline Animation

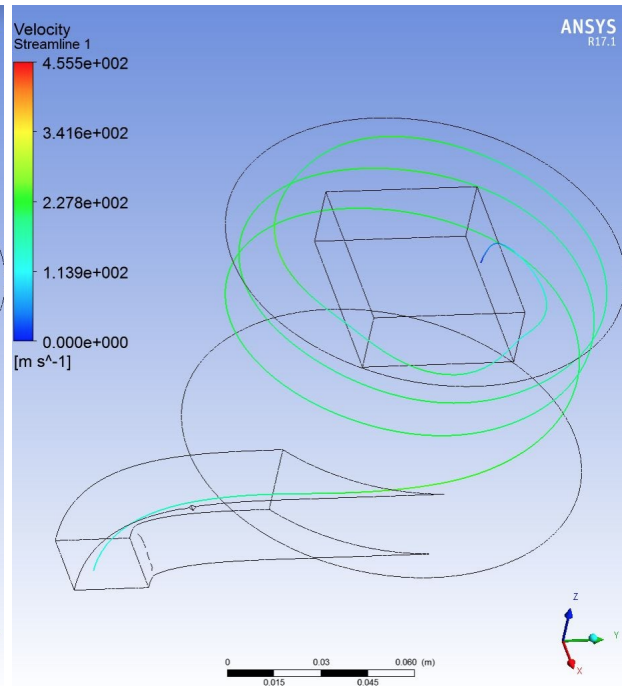


Figure 10. Single Streamline

The left figure above shows a snippet of an animation of the particles traveling along the streamline and the right figure above shows a single streamline. The animation snippet indicates that the air particles do indeed bend around the curve of the dustbin and travel in a vortex. The single line animation shows that the number of rotations a single particle undergoes is roughly three, which validates our calculations in the design section. One caveat to the CFD simulation in general is that only air particles are portrayed since the material listed in the simulation is air only. Dust particles are not considered to be part of this simulation and thus only one vortex is pictured instead of the “double vortex” phenomenon. This is also the reason that dust particle properties were omitted from the velocity and mass flow rate calculations above.

However, a problem arises upon further inspection at the single streamline. The velocity is much higher than the calculated velocity of $31.32 \frac{m}{s}$. The figure below shows more streamlines in the dustbin domain and a mixture and the streamlines show a mix between unexpectedly high velocity (green) and expected low to no velocity due to the boundary condition (shown in blue). The average of the velocities within the dustbin volume domain is $182 \frac{m}{s}$, with a max velocity around $300 \frac{m}{s}$, a magnitude higher than our calculations.

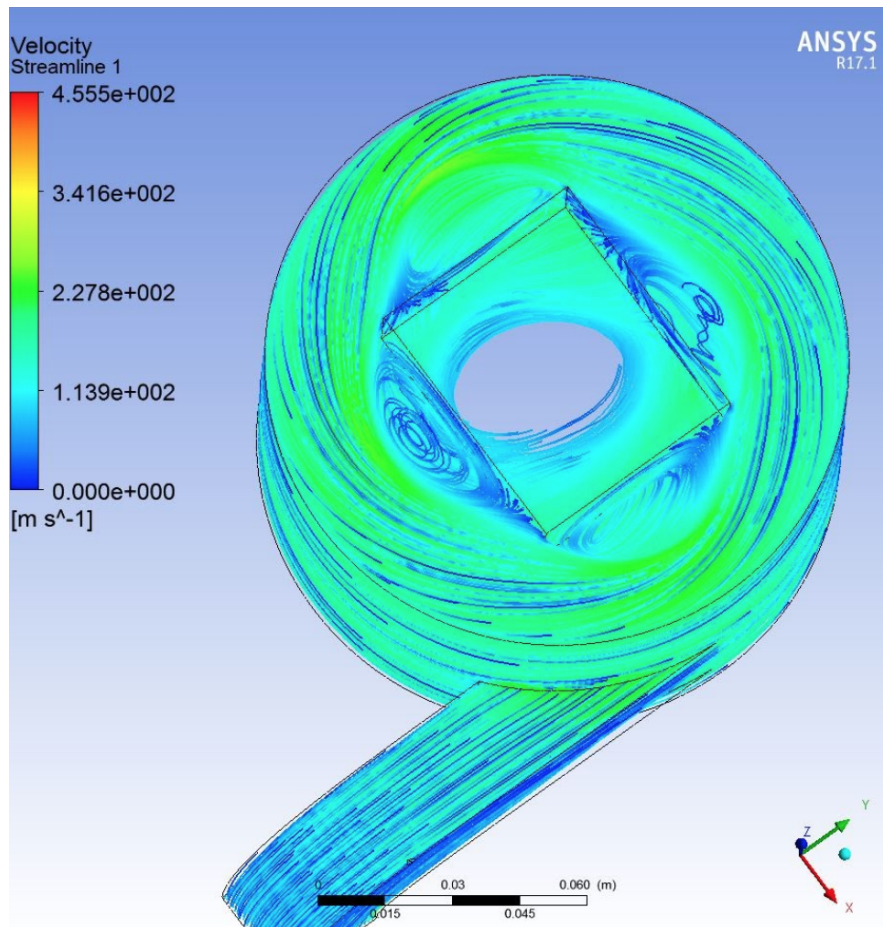


Figure 11. Streamline Velocities

The figure above might give some hints as to why this discrepancy occurs. As the top-down view of the volume domain shows, the radius of the circular trajectories are never small enough for the air to leave through the center portions of the outlet. In fact, roughly a circular area with a diameter equal to the side length of the filter (2in) is not used at all. Subtracting this unused area from the exit area, we obtain a new modified velocity of $72.25 \frac{m}{s}$. Although this velocity is higher than previously calculated, this reasoning alone is still not high enough to explain the velocities generated by CFD. We look to the pressure output shown in the figure below for a further explanation.

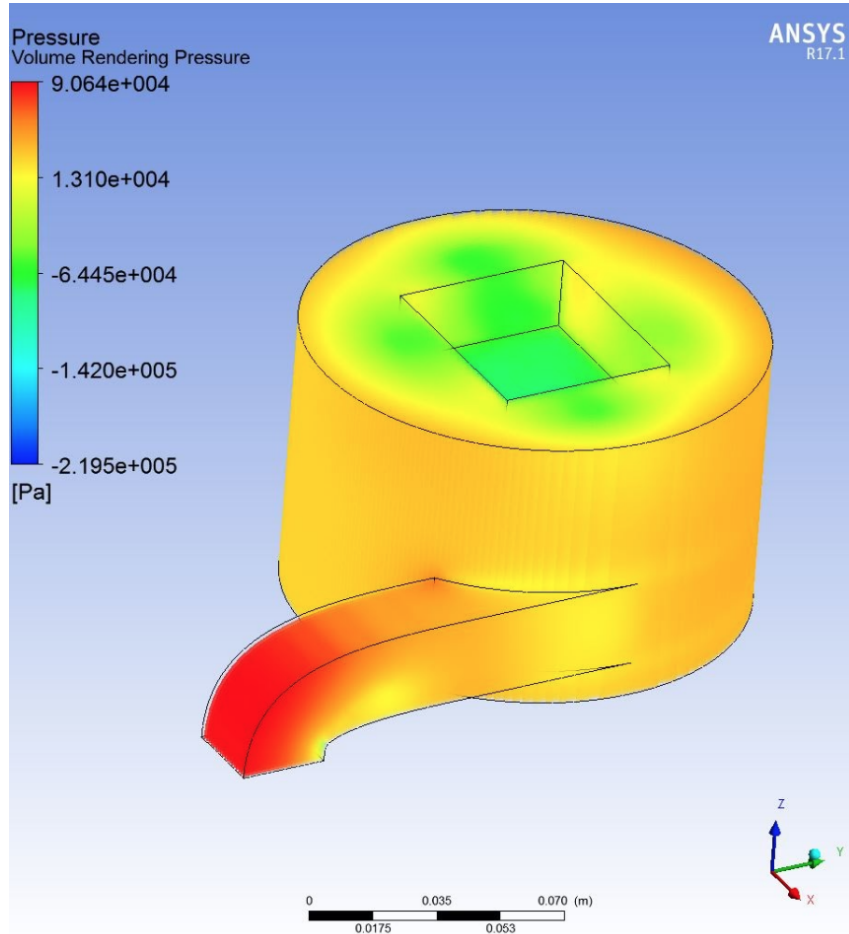


Figure 12. Pressure Gradient

In assumptions listed in the design section, both the inlet and outlet of the vacuum are at atmospheric pressure. However, as the pressure rendering clearly indicated, the inlet is at a significantly higher pressure than the outlet. Accounting for the difference in pressure in the velocity calculation (previously the pressure terms were canceled out and ignored), the newly modified velocity is $321.15 \frac{m}{s}$, which is similar to the velocity outputs.

The geometry of the filter explains why significant back pressure is generated at the outlet. The filter is indented into the volume of the dustbin and only the bottom face of the filter acts as the

outlet. After air travels to the top of the dustbin (where the lid would be), air cannot escape the domain from the topmost surface and instead has to drop down across the height of the filter in order to successfully exit. The process takes time and the rate of the air leaving the domain at the outlet is drastically decreased. The lower mass flow rate means that the velocity of the air leaving the domain will increase according to the conservation of linear momentum, thus creating a pressure drop. This pressure drop creates an adverse pressure gradient that further prevents the air from leaving the outlet. As shown in the streamline figure, the adverse pressure around the side faces of the filter creates smaller vortices on them called recirculation regions. These regions further constrict airflow and as air is trapped inside these regions for longer periods of time, the exit mass flow rate further decreases.

While the reasoning detailed above mentions a decreased mass flow rate which is the streamline animation did seem to portray, the mass flow rate at the outlet output by CFD shows $0.124 \frac{\text{kg}}{\text{ms}}$, which is the value we input assuming the old velocity of $31.32 \frac{\text{m}}{\text{s}}$. This either shows that the thrust needed to generate the desired mass flow rate is much higher than 3N, and the assumptions made to the velocity equation do not capture the real life effects well enough, or the simulation velocity output is still too unreasonably high even with back pressure taken into account. The incorrect simulation output is likely due to insufficient mesh quality, and inaccurate model parameters leading to poor convergence. The continuity residuals output (check on the continuity of mass) of the simulation ran after 2000 iterations only converged to around $1\text{e}-2$, which did not satisfy the criteria of $1\text{e}-6$ I was hoping to achieve.

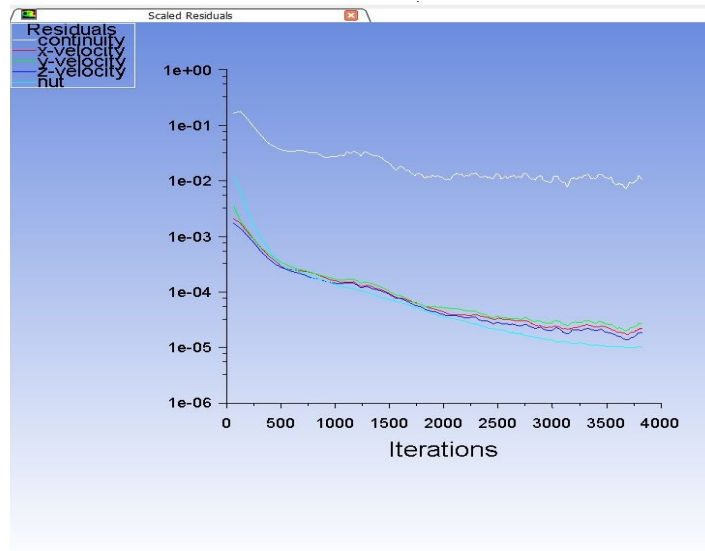


Figure 13. CFD Convergence

Discussion and Conclusion

Although the simulation was not 100% accurate, it is still a good starting off point to validate the design without actually manufacturing and testing it. Although the velocity output is erroneous, other elements of the simulation, such as the general behavior of the air particles and the number of rotations each particle undergoes seemed to correlate well with our hypothesis and hand calculations. The potential increase in expected velocity also does not hurt the performance of the cyclonic vacuum - if anything, a higher velocity means the cyclone is better at separating even the finest dust particles from the air intake. However, if this increased velocity comes at the expense of mass flow rate, this means that the suction rate ability of the vacuum is decreased. Too low of a mass flow rate is detrimental because the nozzle will need to point in one location for a prolonged period of time before all dust can be collected, meaning the robotic platform will take longer for household cleaning applications.

We can modify the simulation by refining the qualities of mesh or fitting different models such as the k-epsilon turbulence model, which is the most common model used in CFD. One attempt has been made to run the simulation using k-epsilon model, but since this model has more equations and Spalart-Allmaras, the computer used ran out of memory before the simulation could finish solving. To reduce memory used, the mesh should be changed to have fewer number of elements without decreasing the mesh quality.

The design and the vacuum could also be improved, specifically the size of the placement of the filter. Since the effective outlet area of the filter is smaller than the actual area, the filter will clog up at a higher rate than expected. This means that the filter will need to be more frequently replaced, which is costly, and the performance of the vacuum will be more frequently affected by the filter. The most direct way to alleviate the problem is use a filter with smaller dimensions to begin with to allow for a decrease in the radius of the dustbin body or make custom filters if off-the-shelf filters have standard dimensions. Alternative methods are to look into moving the filter location to the size and thinking of a way to direct the flow from the filter to the fan, or to have a dustbin with a trapezoidal/conic cross section that is smaller on the top and larger on the bottom so the flow of air will be tighter on top.

References

- [1] Energyeducation.ca. 2020. *Cyclone Separator - Energy Education*. [online] Available at: <https://energyeducation.ca/encyclopedia/Cyclone_separator> [Accessed 8 May 2020].
- [2] Ganegama Bogodage, S. and Leung, A., 2015. CFD simulation of cyclone separators to reduce air pollution. *Powder Technology*, 286, pp.488-506.
- [3] Lauga E., Brenner M., Stone H. (2007) Microfluidics: The No-Slip Boundary Condition. In: Tropea C., Yarin A.L., Foss J.F. (eds) Springer Handbook of Experimental Fluid Mechanics. Springer Handbooks. Springer, Berlin, Heidelberg
- [4] Dartmouth.edu. 2020. [online] Available at: <<http://www.dartmouth.edu/~cushman/courses/engs37/Cyclones.pdf>> [Accessed 8 May 2020].
- [5] Grc.nasa.gov. 2020. *General Thrust Equation*. [online] Available at: <<https://www.grc.nasa.gov/www/k-12/VirtualAero/BottleRocket/airplane/thrsteq.html>> [Accessed 8 May 2020].
- [6] Bergman, T., Lavine, A. and Incropera, F., n.d. *Fundamentals Of Heat And Mass Transfer*. 7th ed.
- [7] Parnell, C., Jones, D., Rutherford, R. and Goforth, K., 1986. Physical properties of five grain dust types. *Environmental Health Perspectives*, 66, pp.183-188.
- [8] Who.int. 2020. [online] Available at: <https://www.who.int/occupational_health/publications/en/oehairbornedust3.pdf> [Accessed 8 May 2020].